

## Accepted Manuscript

A modelling technique for calculating stress intensity factors for structures reinforced by bonded straps. Part I: Mechanisms and formulation

M. Boscolo, X. Zhang

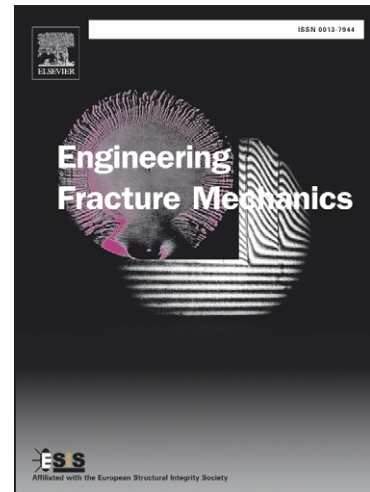
PII: S0013-7944(10)00027-5  
DOI: [10.1016/j.engfracmech.2010.01.013](https://doi.org/10.1016/j.engfracmech.2010.01.013)  
Reference: EFM 3164

To appear in: *Engineering Fracture Mechanics*

Received Date: 18 December 2008  
Revised Date: 7 August 2009  
Accepted Date: 21 January 2010

Please cite this article as: Boscolo, M., Zhang, X., A modelling technique for calculating stress intensity factors for structures reinforced by bonded straps. Part I: Mechanisms and formulation, *Engineering Fracture Mechanics* (2010), doi: [10.1016/j.engfracmech.2010.01.013](https://doi.org/10.1016/j.engfracmech.2010.01.013)

This is a PDF file of an unedited manuscript that has been accepted for publication. As a service to our customers we are providing this early version of the manuscript. The manuscript will undergo copyediting, typesetting, and review of the resulting proof before it is published in its final form. Please note that during the production process errors may be discovered which could affect the content, and all legal disclaimers that apply to the journal pertain.



# A modelling technique for calculating stress intensity factors for structures reinforced by bonded straps.

## Part I: Mechanisms and formulation

M. Boscolo<sup>a,1</sup>, X. Zhang<sup>a,\*</sup>

<sup>a</sup>*Department of Aerospace Engineering, Cranfield University, Bedfordshire, MK43 0AL, UK*

---

### Abstract

This paper describes a 2D FE modelling technique for predicting fatigue crack growth life of integral structures reinforced by bonded straps. This kind of design offers a solution to the intrinsic lack of damage tolerance of integral structures. Due to the multiple and complex failure mechanisms of bonded structures, a comprehensive modelling technique is needed to evaluate important design parameters. In this Part I of a two-part paper, the actions and mechanisms involved in a bonded structure are discussed first, followed by presenting the modelling approaches to simulate each mechanism. Delamination or disbond of the strap from the substrate is modelled by computing the strain energy release rate on the disbond front and applying a fracture mechanics criterion. Thermal residual stresses arising from the adhesive curing process and their redistribution with the substrate crack growth are calculated and taken into account in the crack growth analysis. Secondary bending effect caused by the un-symmetric geometry of one-sided strap is also modelled. In the classic linear elastic fracture mechanics, a non-dimensional stress intensity factor, i.e. the geometry factor  $\beta$ , depends only on the sample's geometry. This  $\beta$  factor cannot be found for this kind of bonded structures, since the magnitude of disbond is related to the applied stress and the disbond size modifies the geometry of the structure. Moreover, secondary bending effect is geometric non-linear thus the stress intensity factor cannot be normalised by the applied stress. For these reasons an alternative technique has been developed, which requires calculating the stress intensity factors at both the maximum and minimum applied stresses for each crack length. This analysis technique is implemented in a computer program that interfaces with the NASTRAN commercial code to compute the fatigue crack growth life of strap reinforced structures.

*Key words:* bonded straps, selective reinforcements, fatigue crack growth life, thermal residual stress, delamination, disbond, secondary bending, bonded patch repair.

**Nomenclature**

$a$	crack length
$E$	Young's modulus
$F_s$	constraint force at crack-tip
$G_{IF}, G_{IM}$	strain energy release rate (mode I) due to traction and bending
$G_{I_{tot}}, G_{I_{mean}}$	total and mean through-thickness strain energy release rate (mode I)
$K_{IF}, K_{IM}$	stress intensity factors due to traction and bending
$K_{IRMS}, K_{IW}$	root-mean-square and weighted through-thickness average stress intensity factors
$K_{app}, K_{res}, K_{tot}$	stress intensity factors due to applied, residual, and combined stress fields
$T_C, T_R, T_o$	curing, room and stress-free temperatures
$t_a, t_r, t_s$	thickness of adhesive, reinforcement strap, and substrate
$\alpha_r, \alpha_s$	coefficients of thermal expansion of reinforcement strap and substrate
$\beta$	non-dimensional stress intensity factor
$\sigma_{ys}$	yield strength

**Subscripts**

$a$	adhesive
$r$	reinforcement strap
$s$	substrate
$W$	weighted function solution
$RMS$	root-mean-square solution

**Abbreviations**

CFRP	carbon fibre reinforced plastics
CTE	coefficient of thermal expansion
FCG	fatigue crack growth
FML	fibre-metal laminate
GFRP	glass fibre reinforced plastics
LEFM	linear elastic fracture mechanics
MVCCT	modified virtual crack closure technique
SENT	single edge notch tension (test sample)
SERR	strain energy release rate
SIF	stress intensity factor
TRS	thermal residual stress
UD	unidirectional

\* Corresponding author. Tel.: +44 1234 754621

Email address: [xiang.zhang@cranfield.ac.uk](mailto:xiang.zhang@cranfield.ac.uk) (X. Zhang).

<sup>1</sup> Present address: School of Engineering and Mathematical Sciences, City University London, Northampton Square, EC1V

## 1. Introduction

Integral structures fabricated by machining or welding rather than riveting are very attractive in terms of reduced structural weight and manufacturing cost [1–3]. However, such structures lack the fail safety capability due to the absence of attached stringers or frames. One promising solution to overcome this problem is to use selective reinforcement or bonded straps [4–11] (see Figure 1). Previous work has concluded that these straps provide significant benefit in terms of reduced crack growth rates and improved fail safety. Heinimann et al. [5] tested different strap configurations and materials, such as the GLARE-1 (glass fibre polymer based fibre metal laminate), aluminium 7075-T762, and carbon fibre polymer based fibre metal laminate, on aluminum substrates and obtained encouraging results in terms of much retarded crack growth rates. For example, wide panels with bonded GLARE straps were tested. Straps were stretched prior to bonding to reverse the thermal residual stresses in the substrate from tension to compression. The thinnest test panels had the largest reinforcement volume fraction (28%) and achieved an average fatigue life improvement of more than 300%. Other test were carried out on aluminum panels reinforced by GLARE or unidirectional (UD) carbon fibre reinforced polymer (CFRP) based fiber metal laminate (FML). Tensile residual stresses were reduced by pinning the grip ends of the substrate and straps during the cure process. Consequently fatigue crack growth (FCG) life was increased significantly. Colavita et al. [7] and Bowler [8] conducted tests and finite element modelling of CFRP straps on aluminium plates. They showed that curing adhesives at elevated temperature could actually reduce the fatigue life of strapped integral structures compared to the un-reinforced case due to the adverse effect of thermal residual stresses (TRS). However, it is both time consuming and expensive to conduct physical tests at the design stage on a wide range of strap parameters. For the design process, analysis tools and simulation models are required. Zhang and Li [6] used the finite element method (FEM) to model the behaviour of integral skin-stringer panels reinforced by straps made of either UD CFRP or Ti-6Al-4V alloy. A strength-based adhesive failure criterion was used. Based on the numerical simulation, FCG life was significantly improved by both types of straps. Strap bridging effect was identified as the main mechanism for crack growth retardation. Boscolo et al. [9] presented a modelling technique based on fracture mechanics to study reinforced plates cured at room temperature. The methodology was validated against test results and the effect of the strap material (elastic modulus), dimension, and position were examined against the added structural weight and FCG life improvement. It was found that if the adhesive is tough enough and cured at room temperature, the stiffness of the strap, which depends on the dimension and material elastic modulus, is the most important

parameter for FCG life improvement. In addition, a project graph was proposed as a design tool to find the lightest strap to achieve a prescribed life improvement target. In [10,11], Zhang et al. studied different strap materials which were tested on mid-crack tension, M(T), and single edge notch tension, SENT, specimens. The substrates were made of aluminium alloy 2024-T351 or 7085-T7651. The bonded straps were made of four different materials, i.e. CFRP, GFRP, GLARE, and Ti-6V-4Al (Ti-6-4). Adhesives were cured at either the room or elevated temperatures to investigate the effect of thermal residual stresses. The extent of crack retardation benefits, in terms of fatigue crack growth life improvement, was established by both numerical simulation and experimental tests. An effective modelling technique was developed to compute the TRS in the substrate and their effect on the FCG life. However, the effects of secondary bending and non-uniform through-thickness crack profile due to the un-symmetric configuration of one-side strap was neglected. The objective of the work reported in this paper is to further develop the modelling technique by implementing all known mechanisms, which include the positive crack bridging effect and adverse effects by strap disbond failure, secondary bending, and curing at elevated temperature. Section 2 summarises all mechanisms involved in bonded strap reinforced structures; section 3 presents the modelling technique development to take into account of all interactive mechanisms; finally FCG life prediction is reported in section 4. Validation of this modelling technique and demonstration examples are reported in [12].

## 2. Mechanisms working in bonded structures

Failure mechanisms involved in a hybrid structure are complex with multiple failure modes and many influential factors that also interact each other. Figure 1 shows a metallic integral skin-stringer panel (substrate) reinforced by bonded composite material straps. Under cyclic loads, four possible failure modes are identified, i.e. initiation and growth of a lead crack in the substrate, disbond failure in the adhesive interface, delamination damage in composite straps due to free-edge effect or impacts, and cracking in the straps due to notch effect. In order to model these failure modes and predict FCG life of reinforced structures, four mechanisms should be simulated.

### Strap stiffening and bridging effect

This is the only positive mechanism. The stiffening/bridging action reduces crack growth rates. Before the substrate crack enters the strap region, the strap is already effective that acts like a “stiffener” taking and transferring part of the load from the cracked substrate. This is the so-called stiffening effect. When the substrate crack enters and passes the strapped region, the traction forces exerted by the strap decrease

the crack opening displacement and reduce the crack tip stress intensity factor; this action is called crack bridging. The scenario is shown in Figure 2.

– **Disbond failure**

The passing of the lead crack under a strap promotes disbond in the bonding interface. Progressive disbond failure will reduce the effectiveness of strap bridging effect.

– **Secondary bending**

Due to the unsymmetrical configuration of one-side strap, secondary bending is generated at the application of external load. This causes the substrate to bend towards the reinforced side producing higher tensile stresses at the un-reinforced side; consequently, different crack growth rates and curved through-thickness crack front are observed.

– **Thermal residual stresses**

These arise from elevated temperature cure of adhesive bonds and are due to the difference in the coefficients of thermal expansion of the two adherends. For the strap materials used in this work, tensile stresses are produced in the substrate causing increased crack growth rates. TRS also causes secondary bending due to unsymmetrical configuration.

These mechanisms, their effects on FCG rates, and the influential parameters are summarised in Table 1. Both the external load and TRS cause secondary bending, but in opposite directions. Secondary bending produces strong geometric nonlinear effect. Therefore, crack tip stress intensity factors due to the mechanical and thermal stresses cannot be simply summed together; both stresses must be considered simultaneously in one nonlinear FE analysis to determine the overall bending direction and magnitude for each crack length.

### 3. Modelling technique

#### 3.1. *Two-layer-plus-spring model*

3D FE models are able to take account of all 3-dimensional actions present in the problem, but they are time and resource consuming. Moreover, the very thin adhesive layer leads to either element aspect ratio problem or extremely fine mesh, which will require even more computational effort. On the other hand, conventional 2D FE models take much less computing time, but it is more difficult to consider the 3D effects, such as the secondary bending and non-uniform crack profiles. Therefore a novel and enhanced 2D FE model has been developed to study bonded crack retarders taking into account of aforementioned

mechanisms and failure modes.

The modelling technique employs 2D plate elements for the substrate and 2D laminate or plate elements for straps made of composite or metallic. Adhesive is modelled by two rigid elements to represent the adhesive layer thickness and three coincident spring elements to mimic the interlaminar peeling and shear actions. This adhesive model was developed by Tahmasebi [13] for analysis of bonded joints and it is used in this work to simulate the behaviour of the bond interface (see Figure 3). The stiffness of the spring elements ( $K_{az}$ ,  $K_{ax}$ , and  $K_{ay}$ ) along the three directions can be calculated by the following equations:

$$K_{az} = \frac{A_a E_a}{t_a} \quad , \quad K_{ax} = K_{ay} = \frac{A_a G_a}{t_a} \quad (1)$$

where  $A_a$  is the area of the adhesive element (Figure 4),  $E_a$  the adhesive elastic modulus,  $G_a$  the adhesive shear modulus, and  $t_a$  the adhesive thickness.

In order to implement the displacement continuity through the thickness, this model makes use of the multi-point constraint (MPC) equations. Based on the Mindlin [14] plate theory the  $i^{th}$ -nodal displacements for a plate element can be written as:

$$u(z)_i = u_i^o + z\phi_i^y \quad , \quad v(z)_i = v_i^o - z\phi_i^x \quad , \quad w(z)_i = w_i^o \quad (2)$$

where  $u_i^o$ ,  $v_i^o$  and  $w_i^o$  are the membrane nodal displacements in the  $x$ ,  $y$ , and  $z$  direction, respectively,  $\phi_i^y$  nodal rotation around  $y$ -direction, and  $\phi_i^x$  nodal rotation around  $x$ -direction. Assign subscript  $s$  to the displacement of the nodes that belong to the substrate and need to be connected to the adhesive,  $a1$  to the nodes on the bottom of the adhesive,  $a2$  to the nodes on the top of the adhesive, and  $r$  to the nodes that belong to the reinforcement strap (see Figure 3), the MPC equations can be written as:

$$\begin{aligned} u_{a1}^o &= u_s^o + \frac{t_s}{2}\phi_s^y \quad , \quad v_{a1}^o = v_s^o - \frac{t_s}{2}\phi_s^x \quad , \quad w_{a1}^o = w_s^o \\ u_{a2}^o &= u_r^o - \frac{t_r}{2}\phi_r^y \quad , \quad v_{a2}^o = v_r^o + \frac{t_r}{2}\phi_r^x \quad , \quad w_{a2}^o = w_r^o \end{aligned} \quad (3)$$

where the subscripts  $s$ ,  $a1$ ,  $a2$ ,  $r$  indicate the plane to which the nodes belong (see Figures 3 and 6),  $t_s$  and  $t_r$  are the thickness of substrate and reinforcement strap, respectively.

Therefore, the 3D effect can be taken into account and the effects of secondary bending, thermal residual stresses and disbond progression can be computed by using this computational efficient 2D model. Geometric non-linear analysis can also be performed by this model.

### 3.2. Stress intensity factors with secondary bending effect

Linear elastic fracture mechanics is used to calculate the principal parameters that govern the fracture failure. Through the FE analysis and the modified virtual crack closure technique (MVCCT) [15–17], strain energy release rate<sup>2</sup> (noted as SERR or  $G$ ) can be computed for the lead crack in the substrate. In the absence of bending, following equation is used:

$$G_I = -\frac{1}{2\Delta a t_s} F_s^y \Delta v_s = -\frac{1}{\Delta a t_s} F_s^y v_s \quad (4)$$

where,  $\Delta a$  is the crack length increment,  $t_s$  the substrate thickness,  $F_s^y$  the constraint force at the crack tip node, and  $v_s$  the displacement at the node immediately behind the crack tip (see figure 5(a)). From the SERR the SIF can be computed by:

$$K_I = \sqrt{G_I E_s^*} \quad (5)$$

where

$$\begin{aligned} E_s^* &= E_s && \text{(plane stress)} \\ E_s^* &= \frac{E_s}{1 - \nu_s^2} && \text{(plane strain)} \end{aligned} \quad (6)$$

and  $E_s$  is the elastic modulus of the substrate material. The plane strain condition is defined by the ASTM standards [18] as:

$$t_s \geq 2.5 \left( \frac{K_I}{\sigma_{ys}} \right)^2 \quad (7)$$

Due to the secondary bending, a rotation and a constraint moment exist in the substrate (see figure 5(b)), consequently, stress intensity factor (SIF) of the main crack varies along the substrate thickness. Methods to obtain the SIF along the crack front for each crack length have been developed for patch repair problems. Wang and Rose[19–21] showed that a distribution of SIF along the crack front cannot be obtained by calculating the strain energy release rates. They argued that, from an energy point of view, only the total energy can be computed ( $G_I$ ) from the two components of the SERR, one due to traction ( $G_{IF}$ ) and the other one due to bending ( $G_{IM}$ ). Applying the MVCCT the total SERR is:

$$G_{I_{tot}} = G_{IF} + G_{IM} = -\frac{1}{\Delta a t_s} (F_s^y v_s^0 + M_s^x \phi_s^x) \quad (8)$$

where,  $v_s^0$  and  $\phi_s^x$  are nodal displacement and rotation,  $F_s^y$  and  $M_s^x$  nodal constraint force and moment,  $t_s$  the thickness of substrate, and  $\Delta a$  the crack extension size necessary to apply MVCCT (see Figure 5(b)).

<sup>2</sup> Since this subsection concerns the substrate only, for clarity, subscript ( $s$ ) is omitted for SERR ( $G$ ) and SIF ( $K$ ).



From the total strain energy release rate, only the root mean square (RMS) value of the SIF ( $K_{I_{RMS}}$ ) can be calculated:

$$K_{I_{RMS}} = \sqrt{G_{I_{tot}} E_s^*} \quad (9)$$

Sun et al. [22–25] used a different approach and calculated the two SIF components from the corresponding SERR components ( $G_{I_F}$  and  $G_{I_M}$ , see Equation 8):

$$K_{I_F} = \sqrt{G_{I_F} E^*} \quad , \quad K_{I_M} = \sqrt{3G_{I_M} E^*} \quad (10)$$

They then assumed a linear distribution of SIF along the crack front (through the thickness) and obtained:

$$K_I(z) = K_{I_F} + \frac{2z}{t} K_{I_M} \quad (11)$$

Thus, a distribution of SIF along the crack front can be calculated by the energy method and, according to their assumption, the distribution is linear.

The method developed in this work is different from the aforementioned two approaches. Here we attempt to demonstrate that a distribution of the SERR and SIF along the crack front can be calculated by using the Mindlin plate theory (Equation 2) to obtain the constraint force  $F_s(z)$  and displacement  $v_s(z)$  variations along the crack front (see Figure 5(b)):

$$v_s(z) = v_s^0 - z\phi_s^x \quad , \quad F_s(z) = F_s^y - z\frac{12M_s^x}{t_s^2} \quad (12)$$

Substituting equation 12 in 4, the SERR distribution through the thickness can be obtained:

$$G_I(z) = -\frac{1}{\Delta at_s} F_s(z)v_s(z) = -\frac{12M_s^x \phi_s^x}{\Delta at_s^3} z^2 + \left( \frac{12M_s^x v_s^0}{\Delta at_s^3} + \frac{\phi_s^x F_s^y}{\Delta at_s} \right) z - \frac{F_s^y v_s^0}{\Delta at_s} \quad (13)$$

now SIF can be computed by using the following equation:

$$K_I(z) = \sqrt{G_I(z) E^*} = \sqrt{\left[ -\frac{12M_s^x \phi_s^x}{\Delta at_s^3} z^2 + \left( \frac{12M_s^x v_s^0}{\Delta at_s^3} + \frac{\phi_s^x F_s^y}{\Delta at_s} \right) z - \frac{F_s^y v_s^0}{\Delta at_s} \right] E^*} \quad (14)$$

This leads to a parabolic distribution of SERR along the crack front; thus SIF is a square root of the parabola.

It is worth noting that the mean value of the SERR through the thickness ( $G_{I_{mean}}$ ), that can be computed

from equation 13, is actually equal to the total SERR ( $G_{I_{tot}}$ ) that was calculated by Wang and Rose in equation 8:

$$G_{I_{mean}} = \frac{1}{t_s} \int_{-\frac{t_s}{2}}^{\frac{t_s}{2}} G_I(z) dz = -\frac{1}{\Delta a t_s} (F_s^y v_s^o + M_s^x \phi_s^x) = G_{I_{tot}} \quad (15)$$

Moreover, it can be shown that by using the total or mean SERR in equation 5 and making use of equation 15, the RMS value of the SIF is obtained:

$$K_I = \sqrt{G_{I_{tot}} E^*} = \sqrt{\frac{1}{t_s} \int_{-\frac{t_s}{2}}^{\frac{t_s}{2}} G_I(z) E^* dz} = \sqrt{\frac{1}{t_s} \int_{-\frac{t_s}{2}}^{\frac{t_s}{2}} K_I(z)^2 dz} = K_{I_{RMS}} \quad (16)$$

This means that the RMS SIF has an actual physic meaning, i.e. it is the SIF obtained from the total (or through-thickness mean) SERR. Furthermore, if equations 8 and 10 are substituted into equation 11 the following expression is obtained:

$$K_I = \sqrt{-\frac{F_s^y v_s^o}{\Delta a t_s} E^*} + \sqrt{-\frac{12 M_s^x \phi_s^x}{\Delta a t_s^3} z^2 E^*} \quad (17)$$

Comparing equations 17 and 14 it can be seen that these two expressions are not identical and the second cannot be reduced to the first. Although the equations are symbolically different, the difference between the two is close to zero if real case SIF values are calculated by these equations. This proves that the distribution of SERR through the thickness as defined in equation 13 is correct and the SIF distribution through the thickness is almost linear as it should be in order to be consistent with the Mindlin plate theory.

This methodology for calculating the SIF along the crack front was firstly validated by the authors in [26] against 3D FE models for patch repair problems. It was subsequently applied to bonded crack retarder straps with other modelling features described in the following sections and validated in the second part of the this paper [12].

### 3.3. Disbond failure modelling

In this work disbond growth is modelled interactively with the growing crack in substrate. In most of the papers in the open literature on selective reinforcement or patch repair problems, disbond is either not considered [19–21,27,28] or modelled based on prescribed disbond shape and size as a function of the substrate crack length based on experimental observations [7,23–25].

For laminated composites and adhesive joints, empirical laws have been developed to study delamination growth under fatigue loads. These laws link the disbond growth rate  $dl/dN$  to the SERR range ( $\Delta G$ ) using

experimentally correlated material constants, e.g. [29–35]. These laws can be written in a generic form as:

$$\frac{dl}{dN} = f(\Delta G) \quad (18)$$

For example, a simple law was developed by Alderliesten et al. [31], in which the effect of cyclic stress ratio and mixed mode delamination is neglected and only the Paris law region is studied. This law has been proved to be adequate to model delamination damages in the fibre-metal laminate GLARE. More complicated laws have been developed for different adhesives and adherends. For example, Kinloch and Taylor [33] have included the near threshold and critical SERR in their disbond model. Andersons et al. [32] studied the cyclic stress ratio effect. Kardomateaset et al. [34] considered mixed mode loading, and to the authors' best knowledge, Shivakumar et al. [35] developed the most complete law to include all aforementioned effects in a single equation.

Once a material law of disbond growth is chosen and the material constants are known, the next task is to compute the SERR range at the disbond front and integrate the material law to obtain the disbond growth life [33,34]. However, there are limitations in these laws. First, database of material constants for currently used adhesives is not available and the sensitivity of these constants to the analysis result is unknown; consequently all those laws can only be used for the adhesive and adherends that they were specifically developed for. Second, none of them can deal with disbond initiation. In fact, to predict the fatigue life of an adhesive joint, the critical SERR value for the onset of disbond initiation as function of cycle numbers [36] must be known; otherwise an initial disbond damage is assumed to exist in the model and over-conservative prediction could be obtained [33]. Thirdly, these Paris law type equations were obtained from tests under single mode load conditions, whereas for the bonded crack retarder problem disbond usually propagates under mixed mode load. Therefore, although there have been some success in modelling adhesively-bonded joints, these empirical laws are not yet ready for modelling bond strap reinforced structures.

A different approach to model delamination growth was developed by Xie [37,38]. A special finite element consisting of two 8-noded plate elements and three spring elements was implemented into the ABAQUS FE software. SERR was calculated by the modified virtual crack closure technique (MVCCT) inside the special element and the springs of this element will be deleted when a mixed mode failure criterion was satisfied.

Therefore a moving delamination front can be modelled using a fixed mesh.

In the modelling technique presented in this paper disbond growth is modelled by the same idea of Xie's [37,38]. Through the MVCCT, three components of the SERR are computed on the disbond front keeping memory of the direction of propagation for each fracture mode (*I*, *II*, *III*):

$$G_I = -\frac{F_{az}(w_{a2} - w_{a1})}{2\Delta l b_a}, \quad G_{II} = -\frac{F_{ay}(v_{a2} - v_{a1})}{2\Delta l b_a}, \quad G_{III} = -\frac{F_{ax}(u_{a2} - u_{a1})}{2\Delta l b_a} \quad (19)$$

where,  $F_{az}, F_{ay}, F_{ax}$  are the forces in the springs,  $w, v, u$  the displacements of the nodes immediately behind the crack tip, and  $\Delta l b_a$  the area of crack extension by which the crack-tip nodes were released to compute the SERR (see figure 6). Using a mixed mode failure criterion (equation 20), failing elements in the adhesive layer are identified and deleted from the FE model to simulate adhesive disbond growth.

$$\frac{G_I}{G_{IC}} + \frac{G_{II}}{G_{IIC}} \geq 1 \quad (20)$$

where,  $G_{IC}$  and  $G_{IIC}$  are critical strain energy release rates for mode I and mode II [37,39,40].

If any adhesive element has failed, then the disbond front will be updated and another FE analysis is followed to compute the SERR along the new disbond front and, again, the failing adhesive elements will be deleted. This interactive analysis goes on until no spring elements fail, i.e. the final disbond shape is found for the given substrate crack length. This method could be called a “quasi-static” delamination growth analysis, since it does not model the effect of fatigue loads. It must be said, though, that disbond growth in patch repair and bonded crack retarders is mostly due to the high local stresses in the substrate crack tip region due to the “stress singularity” effect rather than fatigue loads. This modelling technique has been validated against experimental tests [9,11].

### 3.4. Computation of thermal residual stresses (TRS)

First, it is necessary to understand how these TRS are generated. In the case of two plates bonded at elevated temperature, the two adherends become bonded when the adhesive is completely polymerised at the curing temperature  $T_C$ . This temperature is usually referred to as the stress free temperature  $T_C = T_o$ , since before reaching the temperature the two adherends are still free to expand and slide over each other. When the assembly is cooled down to room temperature  $T_R$  (i.e. the test temperature), the two adherends will try to contract to the original size, but displacement compatibility has to be maintained at the bonding interface. If the coefficients of thermal expansion (CTE) are different for the two adherends, they will contract at different rate during the temperature drop and that generates the TRS.

For an assembly made of two different isotropic adherends of the same dimensions, the beam theory can be used to derive a closed form solution of TRS ( $\sigma_{res}$ ) in the substrate [41]:

$$\sigma_{res} = \frac{t_r E_r E_s (\alpha_r - \alpha_s) \Delta T}{t_r E_r + t_s E_s} \quad (21)$$

where,  $\Delta T = T_R - T_o$  is the difference between the final room temperature ( $T_R$ ) and the stress-free temperature ( $T_o$ ) or the cure temperature ( $T_C$ ). Analytical solution for TRS have been found also for double-sided orthotropic circular reinforcement bonded to infinite or circular isotropic substrates by Wang et al. [42] by making use of the inclusion method. An analytical solution for one-sided composite repairs has also been found by Wang and Erjavec [43]. This solution takes into account of the bending caused by the TRS. Although these equations are very useful for understanding the influential parameters and for quickly finding values of TRS, FE analyses are necessary for more complex geometries. Furthermore, TRS redistribution with crack propagation and coupling between TRS and applied mechanical load in terms of secondary bending (to be further explained in section 4.1) cannot be accounted for without the use of FEM.

Another attempt in accounting for the thermal residual stress effect on FCG life for patched plates was made by Lena et al. [44] by using the modelling technique developed by Sun et al. [22–25]. In their study the effective curing temperature was found by using different trial temperatures in the FE models to compute different trial FCG lives. The computed lives were compared to the life of a sample test and the effective curing temperature was assumed to be the one which produced the smallest difference with the experimental results. Obviously, this assessing procedure would cancel any possible inaccuracy in the SIF computed by FEM and absorb the test scatter. They found that, although the curing temperature of the adhesive was  $120^\circ C$ , the effective temperature which would cause the FCG prediction to be close to the test result was  $62^\circ C$ . Moreover, the effect of the residual SIF was considered to increase the maximum applied SIF instead of influencing the  $R$ -ratio (see end of section II in [44]) as it is done in the literature [45–47] and reported in section 4.1. This approximation, known by Lena et al. [44] was necessary since a material law for the substrate at different  $R$ -ratios (as the one reported in the second part of the paper [12]) was unavailable. In this study, thermal load FE analyses was performed for each strap configuration by inputting a temperature drop equal to the room temperature ( $T_R$ ) minus the cure temperature ( $T_C$ ):

$$\Delta T = T_R - T_C \quad (22)$$

Care should be taken in modelling the curing process and residual stress redistribution during crack propagation for two reasons. First, thermal and mechanical stresses must be applied simultaneously for reasons to be explained in section 4.1. Second, to perform the mechanical load analysis the FE model must be supported as it is in the fatigue testing. However, if the thermal load analysis is conducted under this boundary condition, thermal residual stresses (TRS) will be generated in the support boundaries of the substrate, i.e. where the specimen is clamped. These TRS are not physically there, since the substrate and reinforcement

strap have already reached the equilibrium condition at the end of the curing process without being fitted on to the test machine. In order not to generate these unrealistic TRS, it is necessary to calculate the equivalent CTE for the reinforcement ( $\alpha_r^*$ ) and substrate ( $\alpha_s^*$ ) as follows:

$$\alpha_r^* = \alpha_r - \alpha_s \quad , \quad \alpha_s^* = \alpha_s - \alpha_s = 0 \quad (23)$$

Therefore the substrate does not get unrealistic deformation, and the relative difference in the CTE between the substrate and reinforcement is the same and the effect of temperature can be taken into account without the influence of boundary conditions. Moreover, the temperature drop will be kept there for each crack length and in this way the redistribution of TRS with a growing crack can be modelled. This modelling technique is validated against test results in [12].

In this study the substrate is made of an aluminium alloy and the straps are made of one of the following materials: CFRP, GFRP, Ti-6A-4V, and GLARE. In each case the CTE of the reinforcement material ( $\alpha_r$ ) is smaller than that of the substrate ( $\alpha_s$ ). This difference causes tensile residual stresses in the substrate that promotes crack opening, thus crack propagation.

#### 4. Computing fatigue crack growth life

Two modelling challenges arise for bonded structures. The first is caused by geometric non-linearity of one-side strap configuration, the other is due to the fact that although a distribution of SIF along the crack front can be obtained by aforementioned 2D method, only one SIF value is needed for each crack profile for calculating the FCG rate and life.

##### 4.1. Geometric nonlinearity and alternate analysis method

Geometric nonlinearity effect arises due to the unsymmetrical configuration. Secondary bending presents on application of the mechanical and thermal loads, which leads to nonlinear force-displacement relation.

In the linear elastic case, to compute the SIF range only one FE analysis is needed for each crack length, for example at the maximum load. Then from the stress ratio  $R = \sigma_{min}/\sigma_{max}$ , SIF at the minimum load  $K_{min} = RK_{max}$  and SIF range  $\Delta K = (1 - R)K_{max}$  can be found. This cannot be done when the problem is geometrically nonlinear because:

$$R = \frac{K_{min}}{K_{max}} \neq \frac{\sigma_{min}}{\sigma_{max}} \quad \text{and} \quad \frac{K_{app}}{\sigma_{app}} \neq \frac{K_{max}}{\sigma_{max}} \neq \frac{K_{min}}{\sigma_{min}} \quad (24)$$

This means that a normalised or non-dimensional SIF (the geometry factor  $\beta$ ) does not exist due to the nonlinearity effect.

In this study this problem is solved by performing a so-called “alternate analysis” of the SIF at the maximum and minimum applied stresses; thus  $K_{max}^{tot}$  and  $K_{min}^{tot}$  are calculated for the cyclic maximum and minimum stresses. This leads to an effective  $R$  ratio, which is different from the nominal stress ratio, and an effective SIF range  $\Delta K$  that is different from the calculation result by the classic LEFM superposition rule. This alternate analysis was applied by the authors for a composite patch repair problem [26].

In the presence of TRS the problem is more complicated, since the TRS also cause secondary bending. Due to the nonlinearity of the problem and coupling effect, the applied stress intensity factor ( $K_{app}$ ) and residual stress intensity factor ( $K_{res}$ ) cannot be simply superimposed (figure 7(a)), i.e.:

$$K_{app+res} \neq K_{app} + K_{res} \quad (25)$$

Thus the classic superposition method [46] used to deal with most other residual stress problems (e.g. welding, cold-working) cannot be used. For example, in welded joints, the superposition method results in that  $\Delta K$  is unaffected by the presence of TRS but the effective  $R$  ratio will change.

The total SIF ( $K^{tot}$ ) that includes the interaction between the mechanically applied and thermal residual stresses (figure 7(b)) must be computed at the maximum and minimum applied load separately, which is referred to as the “alternate analysis” in this work. Thus, the SIF range ( $\Delta K$ ) and effective ( $R$ ) ratio can be calculated as:

$$\Delta K = K_{max}^{tot} - K_{min}^{tot} \quad \text{and} \quad R = \frac{K_{min}^{tot}}{K_{max}^{tot}} \neq \frac{\sigma_{min}}{\sigma_{max}} \quad (26)$$

The magnitude of the interaction between mechanical and thermal stress fields is shown in the second part of this paper [12].

#### 4.2. Thickness effect and equivalent SIF

Although the through-thickness distribution of SIF along the crack tip front can be found by equation 14, only one SIF value is required for each crack profile in a crack growth law. Good candidates included the mean, the maximum and RMS values. The RMS is directly connected to the total strain energy release rate [20]), and Sun et al. [25] showed that the best agreement with test results was obtained using the RMS value. The maximum SIF, i.e. the SIF on the un-reinforced side, could give too conservative life prediction, since the interaction with other SIF values through the thickness is neglected.

Duong and Wang [48] has shown that an over conservative life prediction was obtained by using the maximum SIF, but the RMS value can overestimate the FCG life. They found that for a low bending component the FCG life can be better predicted by  $K_{max}$ , whereas for higher bending moments the  $K_{RMS}$  is a better parameter. Thus an equivalent SIF was proposed as a function of a non-dimensional parameter that represents the repair patch stiffness ratio [48].

Hosseini-Toudeshky and Mohammadi [49] conducted two 3D FE analyses of curved and straight crack fronts. They found that the FCG life can be computed by the simpler 3D FE model with straight crack front (which is equivalent to a 2D FE model where the through thickness distribution of SIF is computed) using an equivalent SIF, which, for each crack length, is a value of SIF in a position along the sample's thickness that depends on the elastic modulus of the plate and repair patch as well as the plate thickness. That position was found to be between  $0.32 \sim 0.37$  of the plate thickness from the un-patched side.

In a similar way, a weight function is developed in this work to take account of the fact that the crack length at the un-reinforced side is dragged back by all other shorter crack lengths, and vice versa for the crack length at the reinforced side. This weight function is based on the argument that the crack front, which by a 2D model has to be a straight line, is actually parabolic [27,28,49]. This 3D effect can be considered by a suitable weight function. Imposing the parabola vertex at the un-reinforced side with the value of 1 and prescribing the value on the reinforced side as 0, a weight function ( $W(z)$ ) is obtained to describe the parabola:

$$W(z) = -\frac{1}{t_s^2}z^2 - \frac{1}{t_s}z + \frac{3}{4} \quad \left(-\frac{t_s}{2} \leq z \leq \frac{t_s}{2}\right) \quad (27)$$

Using the weight function (Equation 27) and SERR distribution through the thickness (Equation 13), a weighted SERR ( $G_{Iw}$ ) can be computed:

$$G_{Iw} = \frac{\int_{-t_s/2}^{t_s/2} W(z)G_I(z)dz}{\int_{-t_s/2}^{t_s/2} W(z)dz} = -\frac{9}{10} \frac{M^0\phi}{\Delta at} - \frac{1}{8} \left( \frac{12M^0v^0}{\Delta at^2} + \frac{\phi F^0}{\Delta a} \right) - \frac{F^0v^0}{\Delta at} \quad (28)$$

Similarly, using Equations 14 and 27, a weighed SIF ( $K_{Iw}$ ) can be calculated.

#### 4.3. Life prediction

Fatigue crack growth rates and lives are predicted by using a material law in terms of the crack growth rate vs. the SIF range at different  $R$ -ratios. These curves can be expressed by either an empirical equation, e.g the Paris' law or NASGRO equation, or on point-by-point basis in tabular data form. They are the



material property, albeit suffer from certain scatters. If no material coefficients are available, then the point-by-point described curves ought to be used. In this case it is necessary to obtain at least two experimentally measured crack growth rate curves for two different  $R$ -ratios. Therefore the curves for other  $R$ -ratios can be obtained by the Harter T-method [50]. These curves are numerically integrated with the calculated stress intensity factor range ( $\Delta K$ ) and effective ( $R$ ) ratio as a function of the crack length ( $a$ ) for each study case to compute the fatigue crack growth (FCG) life. The computer code AFGROW [50] cannot be used to compute the FCG life of this kind of structures, since the effective  $R$  ratio cannot be input as a function of the crack length into the code. The way that AFGROW deals with residual stress effect is by inputting the residual stress field first and then calculating the residual stress intensity factors by either the Gaussian integration or a weight function and then use the superposition method to determine the effective  $R$  ratio within the code. As mentioned in section 4.1 and demonstrated in the second part of the paper [12], for one-side bonded structures, the mechanical and thermal residual stress fields interact each other to produce the so-called effective SIF range and effective  $R$  ratio; hence both stress fields must be considered together to deliver the effective SIF and  $R$  ratio values for each crack length.

For this reason a computer subroutine that takes the calculated  $\Delta K$ ,  $R$  and  $a$  as input data has been implemented in the main computer code described in the next section.

#### 4.4. Computer code

A computer program interfacing the commercial package MSC/NASTRAN has been developed to implement the aforementioned analysis techniques and model the failures in bonded strap reinforced structures. First, the SIF values along the thickness for each crack length at the maximum and minimum applied load are calculated. Second, the RMS and weighted SIF values are calculated through the thickness. Third, the SIF range and effective  $R$ -ratio under cyclic loads are calculated for the two equivalent mean SIF values (RMS and weighted). Finally, FCG rate and life are calculated by integrating a corresponding material crack growth law. The integration is carried out by using the Runge-Kutta algorithm [51] of the fifth order. The computer program flow chart diagram can be found in [9].

## 5. Concluding remarks

A modelling technique has been developed that takes into account of all known mechanisms that affect the fatigue crack growth life of bonded strap reinforced structures. Main modelling features are summarised

below.

(1) Adhesive disbond and progressive failure growth are modelled throughout the life of the lead crack in the substrate. (2) Effect of thermal residual stresses and their redistribution due to crack growth are taken into account in calculating the stress intensity factors. (3) Effect of secondary bending under mechanical and thermal stresses on the through-thickness SIF distribution is calculated by the enhanced 2D FE model. Average through-thickness SIF value is determined by a parabolic weight function to model a curved crack front in thick substrate. (4) Geometric nonlinearity under cyclic loads is dealt with by the “alternate analysis” method that takes into account also the nonlinear interaction between the mechanical and thermal stresses. (5) A computer program is developed for predicting fatigue crack growth life by numerical integration using one of the following empirical laws: the NASGRO equation, the Harter T-method, or tabular crack growth rates data.

This modelling methodology is validated by test results of various configurations and strap materials, which is reported in the second part of the paper [12].

**Acknowledgements.** The authors are grateful to Airbus, Alcoa Inc. and the UK Engineering and Physical Sciences Research Council (through the Cranfield IMRC funding) for providing financial support.

## References

- [1] H. J. Schmidt, C. Voto, J. Hansson, Tango metallic fuselage barrel validation of advanced technologies, in: J. Rouchon (Ed.), Proceedings of the 21<sup>st</sup> Symposium of the International Committee on Aeronautical Fatigue, ICAF, Cepadues Editions, 2001, pp. 273–288.
- [2] H. J. Schmidt, B. Schmidt-Brandecker, Damage tolerance design and analysis of current and future aircraft structure, in: AIAA/ICAS International Air and Space Symposium and Exposition: the next 100 years, Dayton, Ohio, 2003, aIAA 2003-2784.
- [3] M. Pacchione, J. Telgkamp, Challenges of the metallic fuselage, in: 25<sup>th</sup> ICAS conference, Hamburg, 2006.
- [4] J. Schijve, Crack stoppers and arall laminates, Engineering Fracture Mechanics 37 (2) (1990) 405–421.
- [5] M. B. Heinimann, R. J. Bucci, M. Kulak, M. Garratt, Improving damage tolerance of aircraft structures through the use of selective reinforcement, in: Proceedings 23<sup>rd</sup> Symposium of International Committee on Aeronautical Fatigue (ICAF), Hamburg, 2005, pp. 197–208.
- [6] X. Zhang, Y. Li, Damage tolerance and fail safety of welded aircraft wing panels, AIAA Journal 43 (7) (2005) 1613–1623.

- [7] M. Colavita, A. Bowler, X. Zhang, P. E. Irving, Adhesively bonded cfrp straps as fatigue crack growth retarders on aa2024-t3, in: SAMPE 2006, Long Beach, 2006.
- [8] A. Bowler, Crack stoppers and fail safety in integral metal aircraft structure, Master's thesis, Cranfield University, United Kingdom (2005).
- [9] M. Boscolo, G. Allegri, X. Zhang, Design and modelling of selective reinforcements for integral aircraft structures, AIAA Journal 46 (9) (2008) 2323–2331.
- [10] X. Zhang, D. Figueroa-Gordon, M. Boscolo, G. Allegri, P. E. Irving, Improving fail-safety of aircraft integral structures through the use of bonded crack retarders, in: Proceedings 24<sup>th</sup> Symposium of International Committee on Aeronautical Fatigue (ICAF), Naples, 2007.
- [11] X. Zhang, M. Boscolo, D. Figueroa-Gordon, G. Allegri, P. E. Irving, Fail-safe design of integral metallic aircraft structures reinforced by bonded crack retarders, Engineering Fracture Mechanics 76 (2009) 114–133.
- [12] M. Boscolo, X. Zhang, A modelling technique for calculating stress intensity factors for structures reinforced by bonded straps. Part II: Validation, Engineering Fracture Mechanics, Submitted.
- [13] F. Tahmasebi, Software tools for analysis of bonded joints, Tech. Rep. 542, NASA/GSFC (2001).
- [14] R. D. Mindlin, Influence of rotatory inertia and shear on flexural vibrations of isotropic, elastic plates, Journal of Applied Mechanics 18 (1951) 1031–1036.
- [15] E. Rybicki, M. Kanninen, A finite element calculation of stress intensity factors by a modified crack closure integral, Engineering Fracture Mechanics 9 (1977) 931–938.
- [16] I. Raju, Calculation of strain energy release rate with higher order and singular finite elements, Engineering Fracture Mechanics 28 (1987) 251–274.
- [17] R. Krueger, The virtual crack closure technique: history, approach and applications, Report No. 2002-10 NASA/CR-2002-211628, ICASE, ICASE Mail Stop 132C NASA Langley Research Center Hampton (2002).
- [18] Standard test method for plane-strain fracture toughness of metallic materials, E399-90, Annual book of ASTM standards (1993).
- [19] C. H. Wang, L. R. F. Rose, On the design of bonded patches for one-sided repair, in: Proceedings 11<sup>th</sup> International conference on composite materials, Gold Coast, Australia, 1997, pp. 347–356.
- [20] C. H. Wang, L. R. F. Rose, R. Callinan, Analysis of out-of-plane bending in one-sided bonded repair, International Journal of Solids Structures 35 (14) (1998) 1653–1675.
- [21] C. H. Wang, L. R. F. Rose, A crack bridging model for bonded plates subjected to tension and bending, International Journal of Solids and Structures 36 (1999) 1985–2014.
- [22] M. Young, C. T. Sun, On the strain energy release rate for cracked plate subjected to out-of-plane bending moment, International Journal of Fracture 60 (1993) 227–247.
- [23] C. Arendt, C. T. Sun, Bending effects of unsymmetric adhesively bonded composite repairs on cracked aluminum panels, in: Proceedings of the FAA/NASSA symposium on advanced integrity methods for airframe durability and damage tolerance, Pt. 1, Hampton, VA, 1994, pp. 33–48.
- [24] C. T. Sun, J. Klung, C. Arendt, Analysis of cracked aluminium plates repaired with bonded composite patches, AIAA Journal 34 (2) (1996) 369–374.

- [25] J. Klug, S. Maley, C. T. Sun, Characterization of fatigue behavior of bonded composite repairs, *Journal of Aircraft* 36 (6) (1999) 1016–1022.
- [26] M. Boscolo, G. Allegri, X. Zhang, Enhanced 2D modelling technique for single-sided patch patches, *AIAA Journal* 47 (6) (2009) 1558–1567.
- [27] W.-Y. Lee, J.-J. Lee, Fatigue behavior of composite patch repaired aluminum plate, *Journal of Composite Materials* 39 (16) (2005) 1449–1463.
- [28] W.-Y. Lee, J.-J. Lee, Successive 3d fe analysis technique for characterization of fatigue crack growth behavior in composite-repaired aluminum plate, *Composite Structures* 66 (2004) 513–520.
- [29] D. J. Wilkins, J. Eisenmann, R. Camin, W. Margolis, R. Benson, Characterising growth in graphite-epoxy, in: *Damage in composite materials*, 1982, pp. 168–183, aSTM STP 775.
- [30] A. Wang, M. Slomiana, R. Buncinel, Delamination crack growth in composite laminates, in: *Delamination and debonding of materials*, 1985, p. 135167, aSTM STP 876.
- [31] R. Alderliesten, J. Schijve, S. van der Zwaag, Application of the energy release rate approach for delamination growth in glare, *Engineering Fracture Mechanics* 73 (2006) 697–709.
- [32] J. Andersons, M. Hojo, S. Ochiai, Empirical model for stress ratio effect on fatigue delamination growth rate in composite laminates, *International Journal of Fatigue* 26 (2004) 597–604.
- [33] A. J. Kinloch, A. C. Taylor, The use of fracture mechanics techniques to predict the service life of adhesive joints, in: D. R. Moore (Ed.), *The application of fracture mechanics to Polymers, adhesives and composites*, volume 33,ESIS publications, 2003, pp. 187–192.
- [34] G. Kardomateas, A. Pelegri, B. Malik, Growth of internal delamination under cyclic compression in composite plates, *Journal of the Mechanics and Physic of Solids* 43 (6) (1995) 847–868.
- [35] K. Shivakumara, H. Chena, F. Abalib, D. Leb, C. Davis, A total fatigue life model for mode i delaminated composite laminates, *International Journal of Fatigue* 28 (1995) 33–42.
- [36] A. J. Vinciguerra, B. Davinson, J. Schaff, S. L. Smith, Determination of mode ii fatigue delamination toughness of laminated composites, *Journal of Reinforced plastics and composites* 21 (07) (2002) 663–677.
- [37] D. Xie, S. Jr.Biggers, Strain energy release rate calculation for moving delamination front of arbitrary shape based on the virtual crack closure technique. part i: Formulation and validation, *Engineering Fracture Mechanics* 73 (2006) 771–785.
- [38] D. Xie, S. Jr.Biggers, Strain energy release rate calculation for moving delamination front of arbitrary shape based on the virtual crack closure technique. Part II: Sensitivity study on modeling details, *Engineering Fracture Mechanics* 73 (2006) 786–801.
- [39] P. P. Camanho, C. Dàvila, Mixed-mode decohesion finite elements for the simulation of delamination in composite materials, Tech. Rep. TM-2002-211737, NASA (June 2002).
- [40] Z. Kutlu, F. Chang, Modeling compression failure of laminated composites contain multiple through-the-width delaminations, *Composite materials* 26 (3) (1992) 350–387.
- [41] S. Timoshenko, J. N. Goodier, *Theory of elasticity*, McGraw-Hill Book Company, 1997.
- [42] C. H. Wang, A. A. B. L.R.F. Rose, R. Callinan, Thermal stresses in a plate with a circular reinforcement, *International Journal of Solids and Structures* 37 (2000) 4577–4599.

- [43] C. H. Wang, D. Erjavec, Geometrically linear analysis of thermal stresses in one-sided composite repairs, *Journal of Thermal Stresses* 23 (2000) 833–851.
- [44] M. R. Lena, J. Klug, C. T. Sun, Composite patches as reinforcements and crack arrestors in aircraft structures, *Journal of Aircraft* 35 (2) (1998) 318–324.
- [45] G. Glinka, Effect of residual stresses on fatigue crack growth in steel weldments under constant and variable amplitude load, Tech. Rep. STP 677, ASTM (1979).
- [46] D. V. Nelson, Effects of residual stress on fatigue crack propagation, Tech. Rep. STP 776, ASTM (1982).
- [47] G. Servetti, X. Zhang, Predicting fatigue crack growth rate in a welded butt joint: The role of effective R ratio in accounting for residual stress effect, *Engineering Fracture Mechanics* 76 (11) (2009) 1589–1602.
- [48] C. N. Duong, C. H. Wang, On the characterization of fatigue crack growth in a plate with a single-sided repair, *Journal of Engineering, Materials and Technology* 126 (2004) 192–198.
- [49] H. Hosseini-Toudeshky, B. Mohammadi, A simple method to calculate the crack growth life of adhesively repaired aluminum panels, *Composite Structures* 79 (2007) 234–241.
- [50] J. Harter, AFGROW users guide and technical manual, Air Vehicles Directorate, afri-va-wp-tr-2006-xxxx Edition (June 2006).
- [51] J. Butcher, Numerical differential equation methods, John Wiley & Sons, 2004, Ch. Numerical methods for ordinary differential equations, pp. 45–121.

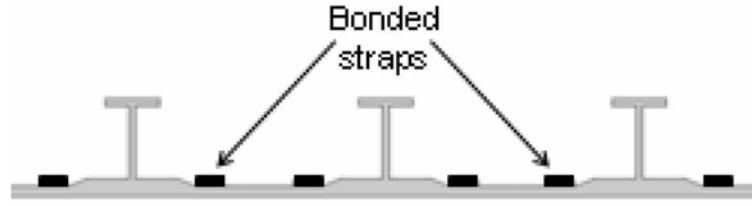


Fig. 1. Schematic of an integral skin-stringer panel with bonded straps

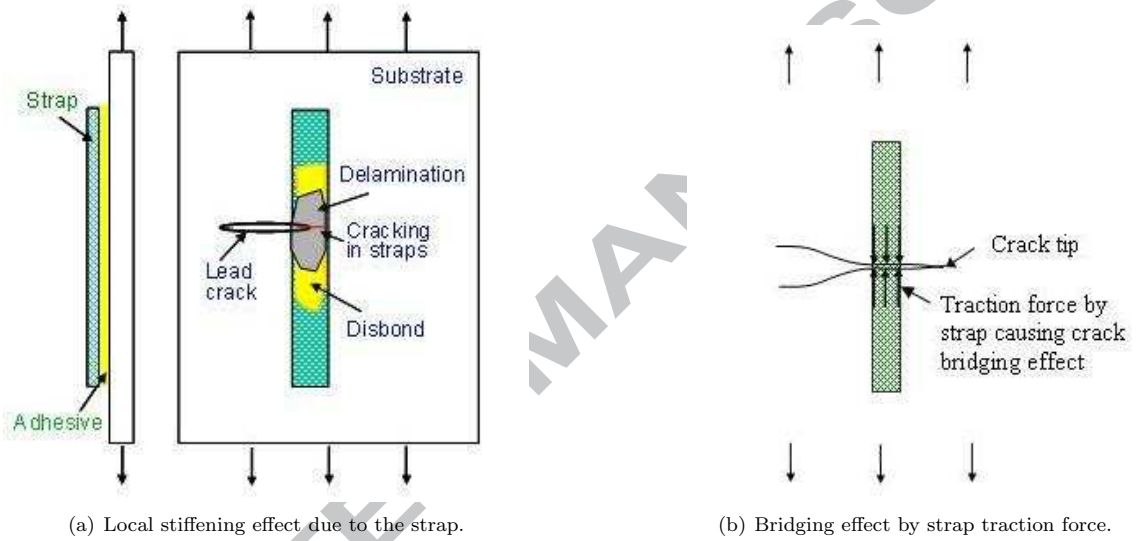


Fig. 2. A bonded structure and four possible damage modes.

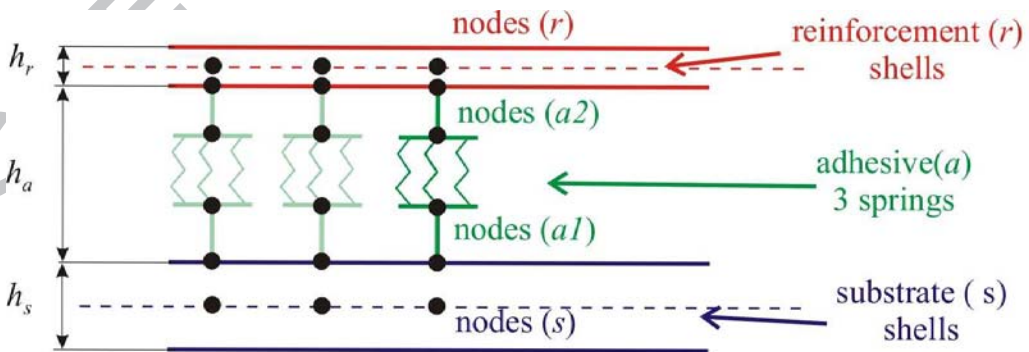


Fig. 3. Diagram of employed finite elements for modelling the substrate plate, reinforcement strap and adhesive. Nodes connecting the "spring" elements are coincident in the model but are shown as detached here for clarity.

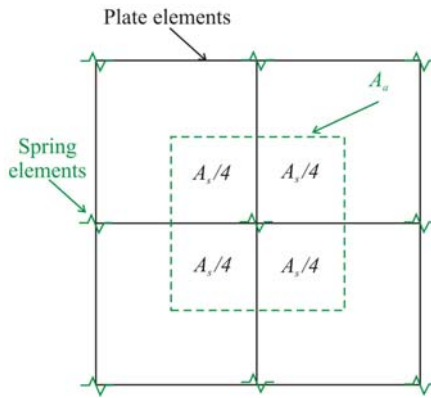
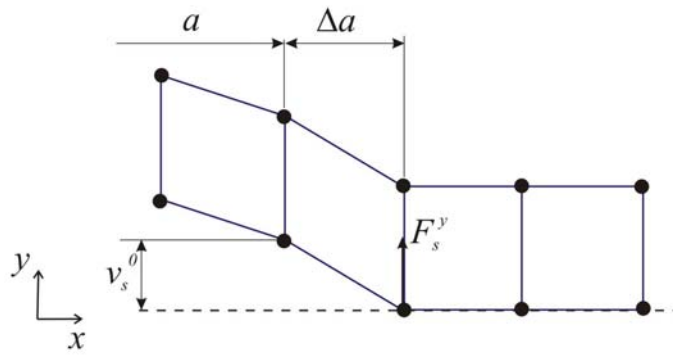
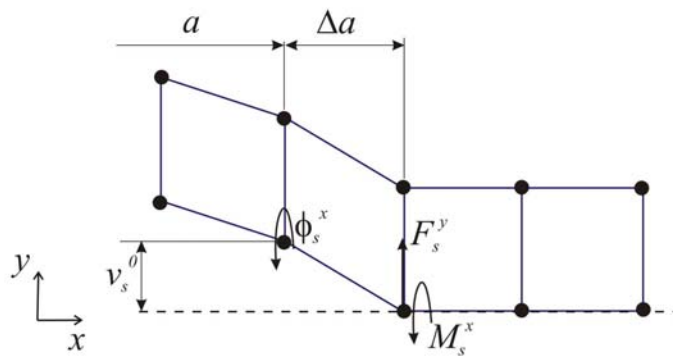


Fig. 4. Area  $A_a$  used for calculating the stiffness of the "spring" element used to model the adhesive.



(a) MVCCT without bending



(b) MVCCT with bending

Fig. 5. Schematic of the modified virtual crack closure technique (MVCCT) for the lead crack in substrate.

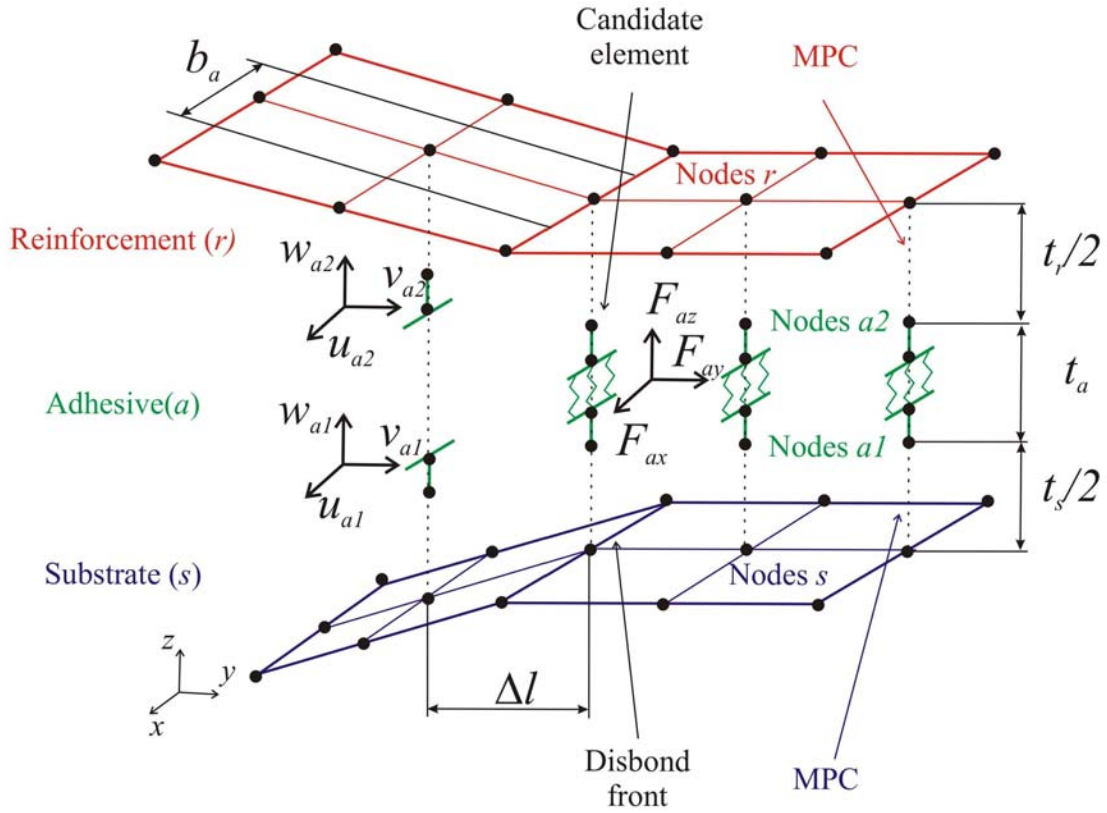
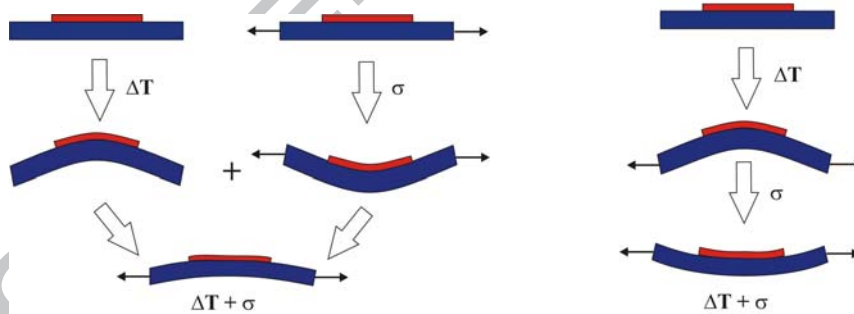


Fig. 6. Schematic of MVCCT for computing the strain energy release rate for candidate spring elements along the disbond front.

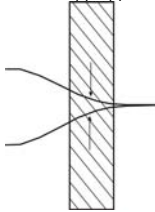
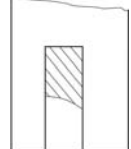




(a) Linear superposition of thermal and mechanical load analyses. (b) Non-linear analysis of thermal and mechanical loads

Fig. 7. Side view sketch of a reinforced plate showing the difference in applying the superposition rule and non-linearity when secondary bending and non-linearity are involved in the problem; the final deformed shapes are different, although the applied thermal and mechanical load are equal.



Table 1  
Summary of mechanisms involved in bonded strap reinforced structures.

	Positive effect	Negative effect		
Mechanism	<p>Stiffening &amp; bridging</p> 	<p>Disbond</p> 	<p>Secondary bending</p> 	<p>Thermal residual stresses</p> 
Description	Reduce crack tip stress and crack opening; slow down crack growth	Reduce the bridging effect	Cause higher crack growth rate and curved crack front	Tensile stresses accelerate crack growth rate
Influential design parameter	<ul style="list-style-type: none"> <li>• Strap stiffness: geometry and mechanical properties</li> </ul>	<ul style="list-style-type: none"> <li>• Adhesive toughness and mechanical properties</li> <li>• Stiffness of strap and substrate</li> </ul>	<ul style="list-style-type: none"> <li>• Plate and strap geometries</li> <li>• Stiffness of strap and substrate</li> </ul>	<ul style="list-style-type: none"> <li>• Plate and strap geometry</li> <li>• Coefficients of thermal expansion               <ul style="list-style-type: none"> <li>• Strap and substrate stiffness</li> <li>• Curing temperature</li> </ul> </li> </ul>